Dalton Transactions

Accepted Manuscript

ROYAL SOCIETY OF CHEMISTRY

www.rsc.org/dalton

Graphical Abstract

Four dinuclear lanthanide complexes $[Ln_2(2\text{-Br-5-MOBA})_6(phen)_2]$ (Ln=Nd(**1**), Sm(**2**), Ho(**3**), Er(**4**); 2-Br-5-MOBA=2-bromine-5-methoxybenzoate, phen=1,10-phenanthroline) have been prepared. The structures of complexes **1** to **4** are isostructural with the coordination number of nine. Heat capacities and thermal circulating processes of the prepared complexes were performed on DSC under nitrogen atmosphere. Two remarkable solid–solid phase transitions existed both in the heat capacities and thermal circulating processes. The bacteriostatic activities of the complexes were determined. Besides, the luminescent property of complex **2** was also performed, and the magnetic properties of complexes **3** and **4** were also discussed.

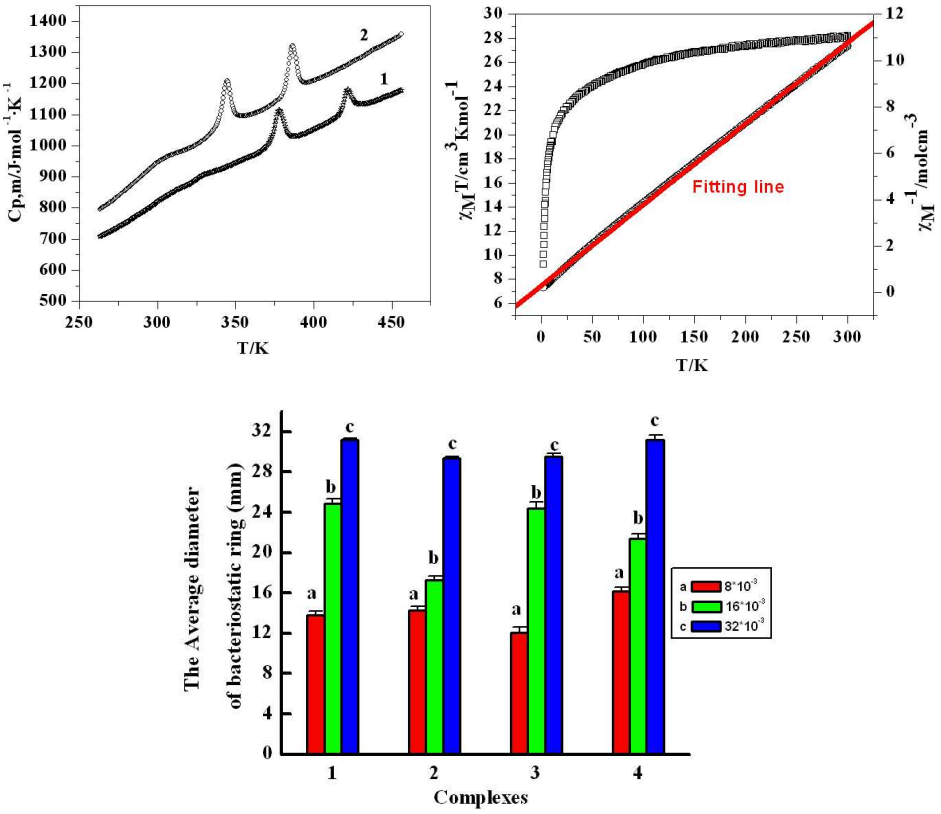

Preparation, characterization and properties of four new trivalent lanthanide complexes constructed by 2-bromine-5-methoxybenzoic acid and 1,10-phenanthroline

Guang-Cai Zong[1,2], Jian-Xia Huo[1,2], Ning Ren[3*], Jian-Jun Zhang[1,2*], Xiao-Xia Qi[1,2], Jie Gao[1,2], Li-Na Geng[2], Shu-Ping Wang[2], Shi-Kao Shi[2]

[1] Testing and Analysis Center, Hebei Normal University, Shijiazhuang 050024 P.R. China.

[2]College of Chemistry& Material Science, Hebei Normal University, Shijiazhuang 050024 P.R. China.

[3]College of Chemical engineering& Material, Handan College, Handan 056005 P. R. China.

Abstract

Four dinuclear trivalent lanthanide complexes of the general formula $[Ln_2(2\text{-Br-5-MOBA})_6(phen)_2]$ (Ln=Nd(**1**), Sm(**2**), Ho(**3**), Er(**4**); 2-Br-5-MOBA = 2-bromine-5-methoxybenzoate, phen=1,10-phenanthroline) were prepared and structurally characterized. The complexes 1 to 4 are isostructural with the coordination number of nine. The carboxylic ligands adopt bridging, bidentate chelating and tridentate chelating bridging modes to coordinate with Ln(III) ions. The structures of the complexes were confirmed on the basis of elemental analysis, molar conductivity, thermogravimetric analysis (TGA), IR and UV spectra. Heat capacities and thermal circulating processes of the prepared complexes were performed on differential scanning calorimeter under nitrogen atmosphere. Two remarkable solid–solid phase transitions existed both in the heat capacities and thermal circulating processes. The bacteriostatic activities of the complexes were evaluated against the *candida albicans*, *escherichia coli* and *staphylococcus aureus*. Besides, the luminescent property of complex **2** was also performed, and the magnetic properties of complexes **3** and **4** were also discussed in detail.

Keywords: 2-bromine-5-methoxybenzoic acid, thermal analysis, solid–solid phase

---

*Corresponding author. Email: ningren9@163.com; Email: jjzhang6@126.com;
Tel.: +86-31180786457 Fax: +86-31180786312

transitions, bacteriostatic activity, magnetic properties

Introduction

Recently, the design of lanthanide complexes containing aromatic carboxylic acids has become the focus of coordination chemistry. [1-4] Lanthanide ions have the unique properties in optical, electrical, and magnetic due to their special electronic structure. The properties can be changed, modified and improved through the interaction between lanthanide ions and carboxylic acid ligands. The study of lanthanide complexes is of fundamental and technological interest due to the diverse structure and potential for wide applications as separation and storage of gas, [5-6] catalyst, [7] electroluminescent, [8-9] biological fluorescence probe [10] as well as magnetic materials.[11-13] Trivalent lanthanide ions are fascinating in fluorescence applications because of their high color purity and relatively long lifetimes associated to the 4f-shell electronic transitions. [14-15] In addition, lanthanide ions have big spin ground state and magnetic anisotropy according to their 4f valence electron spin-orbit coupling effect. So they have great potential in the aspect of design and synthesis of low dimensional molecular magnetic materials. [16] Nowadays, the research of lanthanide complexes in biotechnological fields became more and more important. For instance, the studies of bacteriostatic activities to *candida albicans, escherichia coli,* and *staphylococcus aureus* have been investigated lately.[17-19]

Benzoic acid and some of its derivatives are often used as conservant, catalyst precursor polymers in pharmaceutical industries,[20] which are also used as important organic ligands to construct complexes with lanthanide metal ions.[21-24] On the other hand, the introduction of 1,10-phenanthroline is used mostly as a secondary ligand in lanthanide complexes for good coordination ability which can enhance the stability and luminescent properties of complexes.

Here, we chose 2-bromine-5-methoxybenzoic acid as first ligand and 1,10-phenanthroline as co-ligand to coordinate with Ln(III) ions. Four trivalent lanthanide complexes $[Ln_2(2\text{-Br-5-MOBA})_6(phen)_2]$(Ln=Nd(**1**), Sm(**2**), Ho(**3**), Er(**4**)) were synthesized and characterized by elemental analysis, IR and UV, single crystal X-ray diffraction. Luminescent, bacteriostatic activities and magnetic properties of the

title complexes were also investigated. In particular, two remarkable solid–solid phase transitions were observed in the heat capacities and thermal circulating processes for complexes **1** and **2**. There are few such reports on two solid–solid phase transitions of lanthanide complexes in the process of thermal analysis. [25-26] The results can enrich the contents of rare earth coordination chemistry, and also provide the research basis for the potential applications of the complexes.

Experimental

Materials and methods

$LnCl_3 \cdot 6H_2O$ were prepared by the reaction of Ln_2O_3 (Ln=Nd, Sm, Ho, Er, Beijing Lanthanide Innovation Technology Co., Ltd., Solid, 99.9%) and hydrochloric acid in aqueous solution, followed by recrystallization and drying. Other analytically pure chemicals were purchased and used without further purification.

Equipment and conditions of the experiment

The contents of C, H and N were depicted in Vario-EL II element analyzer and the metal content was obtained by using an EDTA titration method. The molar conductivity was measured by DDS-307 conductivity meter with DMSO as the solvent (Shanghai Precision & Scientific Instrument CO.LED) at room temperature. IR spectrum (4000 - 400 cm^{-1}) were recorded on a Bruker TENSOR 27 spectrometer using KBr pellet technique. Ultraviolet spectra were carried out on a U-3010 Spectrophotometer. The fluorescent spectrum of complex **2** was measured on an F-4500 Hitachi spectrophotometer in the solid state at room temperature.

The single crystal X-ray diffraction data of complexes **1**, **3** and **4** were got on a Smart-1000 (Bruker AXS) diffractometer with monochromated Mo-Kα radiation (λ = 0.71073 Å) at 293, 293, and 298 K, respectively, while the data of complex **2** was obtained with Cu-Kα radiation (λ=1.54178Å) at 298 K. The structures were solved by direct methods using the SHELXS-97 program and refined by full-matrix least-squares on F^2 using the SHELXL-97 program.

Thermogravimetric analysis (TGA) were carried out with products weighing about 3 mg at a heating rate of 10 $K \cdot min^{-1}$(simulated air atmosphere) on a NETZSCH STA

449 F3 instrument. Heat capacities and thermal circulating processes of the prepared complexes were performed on a NETZSCH DSC 200 F3(nitrogen atmosphere) by an indirect measurement method. [27] The temperature and sensitivity calibrations of the instrument of DSC have been checked regularly. They can be calibrated with the melting points and the fusion heats of five standard materials (KNO_3, Hg, Bi, Sn, and CsCl) in the instrument measuring temperature range. Thus, two curves of temperature deviation and sensitivity coefficient can be obtained varying with temperature by curve fitting.

The variable-temperature magnetic susceptibilities were measured on an American Quantum Design MPMS XL7 magnetometer in the temperature range from 2 to 300 K with an applied magnetic filed of 1000 Oe.

Synthesis of the complexes 1 to 4

2-Bromine-5-methoxybenzoic acid (2-Br-5-MOHBA, 3×10^{-4} mol) and 1,10-phenanthroline(1×10^{-4} mol) were together dissolved in ethanol solution (95%). The pH of the ethanol solution was adjusted to in a range of 5-7 by adding 1mol·L^{-1} NaOH solution. The resulting solution of the ligands was then added dropwise into the aqueous solution of $LnCl_3\cdot6H_2O$(1×10^{-4} mol) under stirring. The mixture solution was stirred for 40 min, and then the final turbid solution was sealed in a Teflon-lined autoclave and heated at 120 ℃ for 72h.[28-29] The colorless single crystals suitable for X-ray diffraction analysis were obtained after cooling to the room temperature, Calcd(%) for $C_{72}H_{52}Br_6N_4Nd_2O_{18}$: Nd, 14.22; C, 42.62; H, 2.58; N, 2.76. Found(%): Nd, 14.03; C, 42.34; H, 2.62; N, 2.71. Calcd(%) for $C_{72}H_{52}Br_6N_4Sm_2O_{18}$: Sm, 14.73; C, 42.36; H, 2.57; N, 2.74. Found(%): Sm, 14.44; C, 41.95; H, 2.59; N, 2.71. Calcd(%) for $C_{72}H_{52}Br_6N_4Ho_2O_{18}$: Ho, 15.93; C, 41.77; H, 2.53; N, 2.71. Found(%): Ho, 15.62; C, 41.85; H, 2.59; N, 2.82. Calcd(%) for $C_{72}H_{52}Br_6N_4Er_2O_{18}$: Er, 16.12; C, 41.67; H, 2.53; N, 2.70. Found(%): Er, 16.47; C, 41.74; H, 2.55; N, 2.74.

Results and discussion

Molar conductance

Molar conductivity of the complexes was determined in DMSO with DMSO as a

reference. The values of molar conductivity of complexes **1** to **4** are shown in Table 1. They are all less than 40($S \cdot cm^2 \cdot mol^{-1}$) ,so it can be concluded that complexes **1** to **4** are nonelectrolyte in DMSO.[30] Besides, the molar conductivity decreased with the increase of atomic number from Nd(**1**) to Er(**4**). We speculated that might be explained by the results of the lanthanide contraction. Lanthanide ions radius decreased (from Nd^{3+} to Er^{3+}) as the atomic number increased (from Nd to Er) leading to the trend.

Table 1 Molar conductivity of complexes **1** to **4**

	Complexes	Molar conductivity($S \cdot cm^2 \cdot mol^{-1}$)
1	$[Nd_2(2\text{-Br-5-MOBA})_6(phen)_2]$	29.70
2	$[Sm_2(2\text{-Br-5-MOBA})_6(phen)_2]$	28.60
3	$[Ho_2(2\text{-Br-5-MOBA})_6(phen)_2]$	28.10
4	$[Er_2(2\text{-Br-5-MOBA})_6(phen)_2]$	28.00

Infrared spectra

The important stretching frequencies of the IR spectra of complexes **1** to **4** and two ligands are described in Table 2. As shown in Table 2, the $\nu_{C=O}$ (-COOH) stretching frequency of the organic carboxylic ligand at 1700 cm^{-1} is absent in the IR spectra of complexes **1**-4, whereas the characteristic bands for $\nu_{as}(C=O)$ and $\nu_{s}(C=O)$ are observed at 1635-1618 cm^{-1} and 1428-1419 cm^{-1}, respectively. The absorption peaks in the region 417-419 cm^{-1} show the typical vibrations of Ln – O. They indicate the carboxyl groups of the benzoate are coordinated to Ln(III) ions by a proton released.[31] In addition, the $\nu_{C=N}$ of 1,10-phenanthroline at 1561cm^{-1} shifts to1558-1552 cm^{-1} in the complexes. The δ_{C-H} at 854 cm^{-1},736 cm^{-1} of 1,10-phenanthroline shift to 842-840 cm^{-1} ,730-727 cm^{-1} in the complexes, which reveal two nitrogen atoms of the 1,10-phenanthroline are also coordinated to Ln(III) ions.[26]

Table 2 The characteristic absorbing bands of ligands and complexes **1** to **4**

Ligands/Complexes	$\nu_{C=N}$	$\nu_{C=O}$	$\nu_{as(COO^-)}$	$\nu_{s(COO^-)}$	δ_{C-H}	$\nu_{(Ln-O)}$
1,10-phenanthroline	1561				854，736	
2-Br-5-MOHBA		1700				
1	1552		1618	1422	842，730	417
2	1555		1620	1428	840，730	419
3	1558		1632	1419	840，727	417
4	1555		1635	1422	840，730	419

Ultraviolet Spectra

The UV spectra of ligands phen, 2-Br-5-MOHBA as well as complexes in dimethyl sulfoxide (DMSO) solution ($c=1\times10^{-5}$ mol·L^{-1}) are determined with DMSO as reference. As shown in Table 3, the absorption peak of 2-Br-5-MOHBA ligand at 257 nm shifts to 261 to 267 nm in the complexes, indicating that the carboxylic acid ligands are coordinated to the lanthanide ions forming a π-conjugated system. [31] Compared with the λ_{max} of 1,10-phenanthroline, there is no obvious shift in the complexes, suggesting that the formation of Ln-N has no significant influence on ultraviolet absorption of 1,10-phenanthroline. However, the values of A_{max} of complexes are all stronger than those of two ligands. This may be the explanation that a larger chelate ring is constructed after coordinating with the Ln(III) ions. [33]

Table 3 The absorption peaks of ultraviolet spectra of ligands and complexes **1** to **4**

Ligands/Complexes	λ_{max}(nm)	A_{max}
1,10-phenanthroline	265	0.31
2-Br-5-MOHBA	257	0.09
1	266	0.98
2	261	1.20
3	265	0.91
4	262	1.25

Crystal structures of the complexes

The detailed crystallographic data of the complexes are listed in Table 4, and the selected bond lengths are listed in Table 5. The determination of X-ray single crystal structures show that complexes **1** to **4** are isostructural and they are all binuclear molecules containing two 1,10-phenanthroline molecules, six 2-bromine-5-methoxybenzoate and two Ln(III) ions. Here, the crystal structure of complex **2** will be described in detail. The molecular structure of complex **2** and the coordination geometry of the Sm(III) ion are shown in Fig. 1. The crystal structures of complexes **1**, **3** and **4** are shown in Fig. S1-S3. As shown in Fig.1, the carboxylic groups adopt bridging, bidentate chelating and tridentate chelating bridging modes to coordinate Sm(III) ions. [34] The nitrogen atoms of 1,10-phenanthroline are coordinated to

Sm(III) ions via bidentate chelating mode. Each Sm(III) ion is nine-coordinated by seven oxygen atoms from six 2-Br-5-MOBA ligands and two nitrogen atoms from one phen molecule. The coordination sphere of Sm(III) ion can be described as a distorted mono-capped square antiprism. The atom O4A occupies the cap position of the polyhedron and atoms O4, O2A, O5A, O_1 and O7, O8, N1, N2 construct the upper and lower planes, respectively. [35] The length of Sm-O is in the range from 2.340(14) Å to 2.694(13) Å and the average bond length is 2.464(85) Å. The length of Sm(1)-O(4)A is the longest because the cap position of O(4)A leads to the bond length of growth. The average bond length for Sm-N was 2.631(68) Å，which is longer than 2.464(85) Å of Sm-O due to the stronger coordination ability of the oxygen atoms.[36] It can be confirmed that 1,10-phenanthroline ligand is lost firstly in the thermal decomposition process. In total, the average lengths of Ln-N of complexes from **1** to **4** were gradually reduced with the atomic number increased, which could be explained by lanthanide contraction.

Table 4 Single crystal data and structure refinement for the complexes **1** to **4**

	Complex **1**	Complex **2**	Complex **3**	Complex **4**
Empirical formula	$C_{72}H_{52}Br_6N_4Nd_2O_{18}$	$C_{72}H_{52}Br_6N_4Sm_2O_{18}$	$C_{72}H_{52}Br_6Ho_2N_4O_{18}$	$C_{72}H_{52}Br_6Er_2N_4O_{18}$
Formula weight	2029.12	2041.34	2070.5	2075.16
Temperature(K)	293(2)	293(2)	298(2)	298(2)
Wavelength(Å)	0.71073	1.54178	0.71073	0.71073
Crystal system	Triclinic	Triclinic	Triclinic	Triclinic
space group	Pī	Pī	Pī	Pī
a(Å)	12.4699(12)	12.4625(11)	12.3030(11)	12.3319(13)
b(Å)	13.2334(13)	13.2328(12)	13.0809(12)	13.0886(14)
c(Å)	13.5944(13)	13.5772(14)	13.1291(14)	13.1255(11)
α(°)	61.1050(10)	60.8420(10)	61.6480(10)	61.5350(10)
β(°)	69.682(2)	69.7760(10)	74.2230(10)	74.3260(10)
γ(°)	71.280(2)	71.198(2)	77.406(2)	77.266(2)
Volume (Å^3)	1809.5(3)	1802.1(3)	1779.5(3)	1782.6(3)
Z, Calculated density(Mg•m^{-3})	1, 1.862	1, 1.881	1, 1.932	1, 1.933
Absorption coefficient(mm^{-1})	4.804	16.617	5.649	5.774
F(000)	986	990	1000	1002
Crystal size (mm)	0.12 x 0.10 x 0.09	0.21 x 0.09 x 0.05	0.32 x 0.21 x 0.13	0.21 x 0.08 x 0.04
Theta range for data collection (°)	2.74 to 25.02	3.83 to 66.03	2.73 to 25.02	2.61 to 25.02

Limiting indices	-14≤*h*≤14	-14≤*h*≤14	-12≤*h*≤14	-13≤*h*≤14
	-15≤*k*≤12	-15≤*k*≤15	-15≤*k*≤14	-14≤*k*≤15
	-16≤*l*≤16	-10≤*l*≤16	-14≤*l*≤15	-8≤*l*≤15
Reflections collected /	11888 / 6380	11012 / 6273	8892 / 6149	8798 / 6124
unique	[$R_{(int)}$ = 0.1207]	[$R_{(int)}$ = 0.1154]	[$R_{(int)}$ = 0.0496]	[$R_{(int)}$ = 0.0854]
Completeness to theta =				
25.02	99.90%	99.80%	97.80%	97.30%
Max. and min.				
transmission	0.6717 and 0.5964	0.4904 and 0.1281	0.5271 and 0.2651	0.8019 and 0.3769
Data / restraints /				
parameters	6380 / 0 / 463	6273 / 0 / 464	6149 / 0 / 463	6124 / 0 / 464
Goodness-of-fit on F^2	0.981	1.028	1.019	1.003
Final *R* indices [$I>2\sigma(I)$]	R_1 = 0.0897	R_1 = 0.0974	R_1 = 0.0654	R_1 = 0.0950
	wR_2 = 0.1175	wR_2 = 0.1717	wR_2 = 0.1516	wR_2 = 0.1936
R indices (all data)	R_1 = 0.1839	R_1 = 0.1749	R_1 = 0.0961	R_1 = 0.1904
	wR_2 = 0.1613	wR_2 = 0.2596	wR_2 = 0.1716	wR_2 = 0.2425
Largest diff. peak and				
hole e.Å^{-3}	1.387 and -1.375	2.140 and -2.143	3.285 and -4.478	2.110 and -2.395

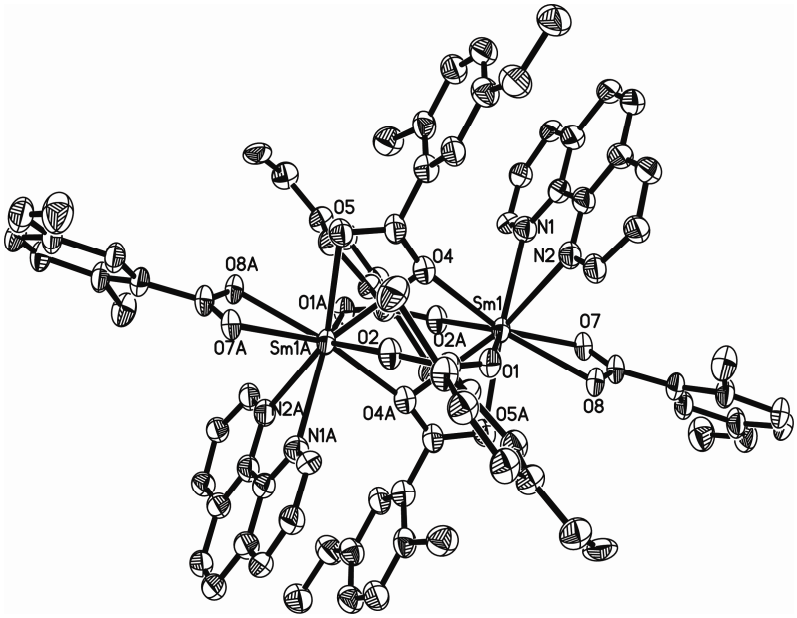

(a)

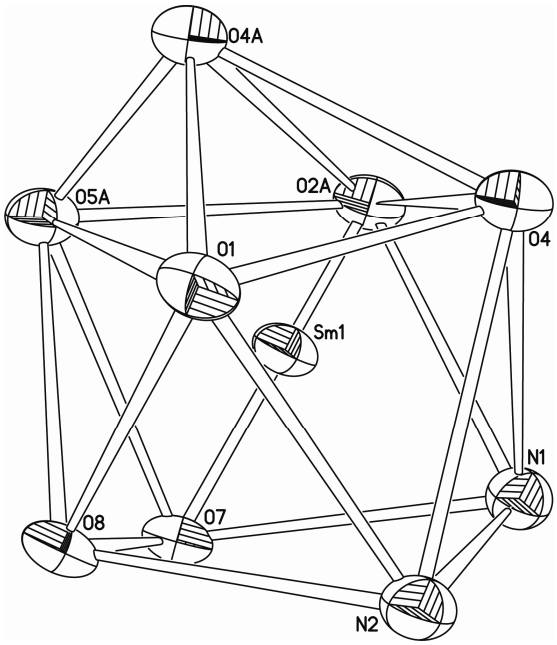

(b)

Fig. 1 The crystal structure of complex **2**(a) and coordination geometry of the Sm(III) ion(b) with non-hydrogen atoms drawn by diamond.

Table 5 The selected bond lengths of complexes **1** to **4**

Complex **1**		Complex **2**		Complex **3**		Complex **4**	
	Bond length (Å)		Bond length (Å)		Bond length (Å)		Bond length (Å)
Nd(1)-O(5)#	2.395(7)	Sm(1)-O(4)	2.340(1)	Ho(1)-O(4)#	2.284(7)	Er(1)-O(1)	2.260(16)
Nd(1)-O(4)	2.405(7)	Sm(1)-O(2)#	2.364(1)	Ho(1)-O(2)#	2.287(7)	Er(1)-O(4)#	2.274(16)
Nd(1)-O(2)#	2.415(7)	Sm(1)-O(1)	2.401(1)	Ho(1)-O(1)	2.316(6)	Er(1)-O(2)#	2.306(14)
Nd(1)-O(8)	2.479(8)	Sm(1)-O(8)	2.466(1)	Ho(1)-O(5)	2.383(7)	Er(1)-O(5)	2.398(14)
Nd(1)-O(7)	2.482(7)	Sm(1)-O(7)	2.467(1)	Ho(1)-O(8)	2.400(7)	Er(1)-O(8)	2.419(13)
Nd(1)-O(1)	2.521(7)	Sm(1)-O(5) #	2.521(1)	Ho(1)-O(7)	2.406(7)	Er(1)-O(7)	2.431(16)
Nd(1)-O(2)	2.719(6)	Sm(1)-O(4) #	2.694(1)	Ho(1)-O(4)	2.869(7)	Er(1)-O(4)	2.894(14)
Average length of Ln-O	2.488(7)		2.464(9)		2.421(4)		2.426(15)
Nd(1)-N(2)	2.641(9)	Sm(1)-N(2)	2.613(2)	Ho(1)-N(2)	2.534(9)	Er(1)-N(2)	2.530(18)
Nd(1)-N(1)	2.669(8)	Sm(1)-N(1)	2.650(2)	Ho(1)-N(1)	2.552(9)	Er(1)-N(1)	2.536(19)
Average length of Ln- N	2.655(9)		2.631(7)		2.543(9)		2.533(19)

Symmetry transformations used to generate equivalent atoms: #1 -x+1,-y+1,-z+1

Thermal analysis

TG-DTG curves of complexes **1**-**4** are recorded at a heating rate of 10 $K \cdot min^{-1}$

under simulated air atmosphere. The profiles of thermal decomposition processes of the title complexes are similar, which are shown in Fig. 2. The thermal analysis data of the specific processes were listed in Table 6. Complex **2** is taken as an example for a detailed analysis. As shown in Fig.2(a), the DTG curve shows mass loss in four steps. The first mass loss between 506.15 K to 667.15 K with a peak temperature of 614.15 K are attributed to the release of 1,10-phenanthroline and part of the 2-Br-5-MOBA ligand (Calc. = 17.65%, TG = 29.51%). The second, third and fourth mass loss of 7.85% , 34.65% and 9.83% between 667.15 and 1149.15 K, are attributed to the loss of the 2-Br-5-MOBA ligand. The complex 2 completely collapsed into the final product of Sm_2O_3 .The total weight loss is 81.84%, which is in agreement with the calculated value of 82.91%.

Table 6 The Thermal analysis results of complexes **1** to **4**

Complexes	Steps	Temperature range/K	DTG Tp/K	Mass loss rate/%		Probable expelled groups	Intermediate and Residue
				Found	Calcd		
1	I	506.15-671.15	614.15	31.51	17.76[a]	phen + Part 2-Br-5-MOBA	$[Nd_2(2\text{-Br-5-MOBA})_{6-2x}]$
	II	671.15-766.15	744.15	8.87	--	Part 2-Br-5-MOBA	$[Nd_2(2\text{-Br-5-MOBA})_{6-2x-2y}]$
	III	766.15-938.15	834.15	35.74	--	Part 2-Br-5-MOBA	$[Nd_2(2\text{-Br-5-MOBA})_{6-2x-2y-2z}]$
	IV	938.15-1168.15	1071.15	7.20	65.65[b]	The remaining 2-Br-5-MOBA	Nd_2O_3
				83.32	83.41		
2	I	506.15-667.15	616.15	29.51	17.65[a]	phen +Part 2-Br-5-MOBA	$[Sm_2(2\text{-Br-5-MOBA})_{6-2x}]$
	II	667.15-757.15	745.15	7.85	--	Part 2-Br-5-MOBA	$[Sm_2(2\text{-Br-5-MOBA})_{6-2x-2y}]$
	III	757.15-885.15	804.15	34.65	--	Part 2-Br-5-MOBA	$[Sm_2(2\text{-Br-5-MOBA})_{6-2x-2y-2z}]$
	IV	885.15-1149.15	1027.15	9.83	65.26[b]	The remaining 2-Br-5-MOBA	Sm_2O_3
				81.84	82.91		
3	I	504.15-683.15	613.15	32.61	17.41[a]	phen +Part 2-Br-5-MOBA	$[Ho_2(2\text{-Br-5-MOBA})_{6-2x}]$
	II	683.15-790.15	764.15	8.85	--	Part 2-Br-5-MOBA	$[Ho_2(2\text{-Br-5-MOBA})_{6-2x-2y}]$
	III	790.15-925.15	849.15	31.50	--	Part 2-Br-5-MOBA	$[Ho_2(2\text{-Br-5-MOBA})_{6-2x-2y-2z}]$
	IV	925.15-1156.15	996.15	8.29	64.34[b]	The remaining 2-Br-5-MOBA	Ho_2O_3
				81.25	81.75		
4	I	515.15-670.15	616.15	30.02	17.37[a]	phen +Part 2-Br-5-MOBA	$[Er_2(2\text{-Br-5-MOBA})_{6-2x}]$
	II	670.15-787.15	771.15	9.76	--	Part 2-Br-5-MOBA	$[Er_2(2\text{-Br-5-MOBA})_{6-2x-2y}]$
	III	787.15-899.15	838.15	33.78	--	Part 2-Br-5-MOBA	$[Er_2(2\text{-Br-5-MOBA})_{6-2x-2y-2z}]$
	IV	899.15-1065.15	947.15	7.42	64.20[b]	The remaining 2-Br-5-MOBA	Er_2O_3
				80.98	81.57		

T_p:the peak temperature of DTG,

a: theoretical total weight loss of phen,

b: theoretical total weight loss of 2-Br-5-MOBA.

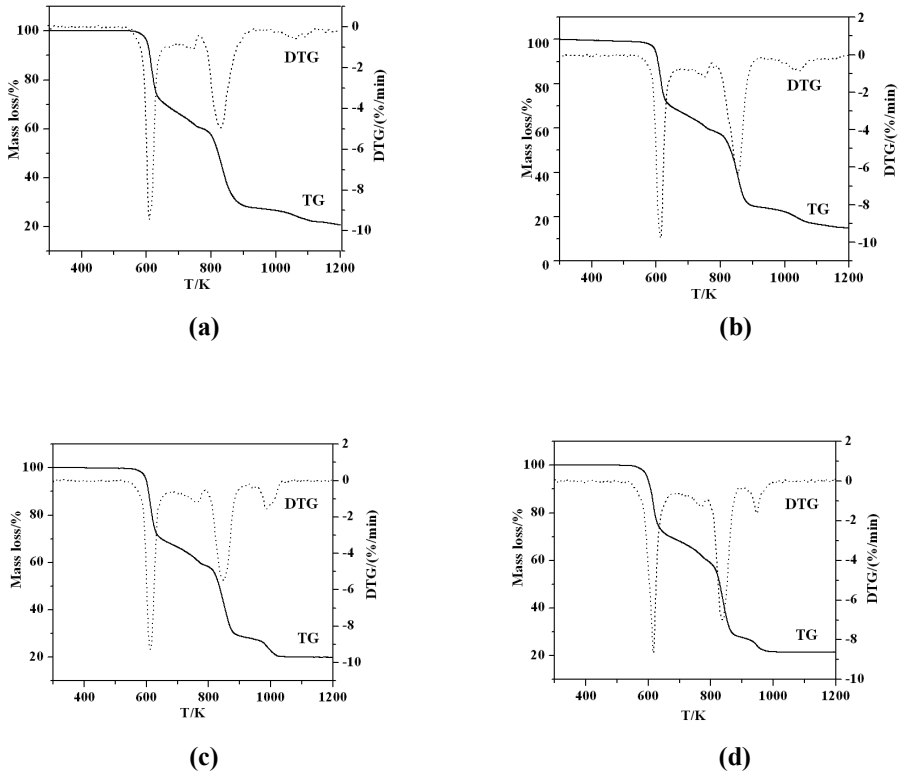

Fig. 2 The TG-DTG curves of complexes **1** to **4**(complex 1= a, complex 2= b, complex 3= c, complex 4= d)

Molar heat capacities of complexes

The molar heat capacities of complexes **1-4** are studied at a heating rate of 10 $K \cdot min^{-1}$ under nitrogen atmosphere by DSC instrument. The highest temperature is 463.15 K because they are stable up to 500 K by thermogravimetric analysis. The relationship of molar heat capacity and temperature of complexes **1-4** are shown in Fig.3. As shown in Fig.3(b), the molar heat capacity values of the complexes 3 and 4 gradually increase with the increase of temperature. It seems that the curve of complex 4 are not smooth at temperature from 300K to 350K.The molar heat capacity values of complex 4 increase rapidly and slowly then, which needs further study. However, as shown in Fig.3(a), there are two obvious endothermic peaks in the curves of complexes 1-2. The results of TG-DTG analysis reveal that there is no mass loss in the temperature range. So we speculate that the endothermic peaks may be attributed to solid–solid phase transitions of the complexes.[25-26] This speculation has been confirmed through further studies. Four thermal circulating processes of complexes **1** and **2** have been

designed with the scanning rate of 10 K·min^{-1} from 263.15 K to 463.15 K. The DSC curves of thermal circulating are described on Fig. 4. There are always two peaks in the heating and cooling processes. The temperature and enthalpy of endothermic and exothermic in each process for complexes **1** and **2** are shown in Table 7. Seen from the Table, the phase transition temperature in cooling process was lower than that in heating process in the same circulating process, which can be explained by the presence of super cooling phenomenon in the thermal circulating processes. However, the value of enthalpy in heating and cooling processes for complexes **1** and **2** are almost no remarkable change. For instance, the value of enthalpy of complex **1** was -0.991 KJ/mol at the first cooling circulation (the first phase transitions process). With the continuing of the circulation, the values of enthalpy are -0.990, -0.893, -0.851 KJ/mol, respectively. So we can conclude that the values of enthalpy of the four circulating processes are essentially unchanged. All these phenomena can confirm that the endothermic and exothermic peaks of complexes 1-2 represent the solid–solid phase transitions.[25]

The average molar heat capacity values of complexes **1**-4 are shown in Table S1 and S2 (see supplementary data), respectively. Fitting the value of average molar heat capacity with the reduced temperature (x) which calculated from the formula $x = [T - (T_{max} + T_{min})/ 2]/[(T_{max} - T_{min})/2]$ by using the least square method, polynomial equations of the complexes were obtained as follows(E was used as a representative of 10^6 in the field of mathematics)

Complex **1** [Nd_2(2-Br-5-MOBA)$_6$(phen)$_2$] (T=263.15 K to 366.65 K)

$C_{p,m}$/J·mol^{-1}·K^{-1}=967.14685+232.92679x+207.10767x^2-347.85674x^3-3797.625x^4-3896.2478x^5+11049.13739x^6+29896.53969x^7+26366.49709x^8+8198.73104x^9

R^2=0.9997 SD= 1.36202

Complex **2** [Sm_2(2-Br-5-MOBA)$_6$(phen)$_2$] (T=263.15 K to 335.65 K)

$C_{p,m}$/J·mol^{-1}·K^{-1}=5784.74207+81231.54222x+610395.89116x^2+2.61308E6x^3+6.96126E6x^4+1.19363E7x^5+1.31749E7x^6+9.04399E6x^7+3.51281E6x^8+589845.87657x^9

R^2=0.9999 SD= 0.34436

Complex **3** [Ho_2(2-Br-5-MOBA)$_6$(phen)$_2$] (T=263.15 K to 456.15 K)

$C_{p,m}$/J·mol^{-1}·K^{-1}=819.78832+165.98735x-4.3597x^2+179.41651x^3+351.5471x^4-431.5755

$8x^5$-789.99559x^6+510.42408x^7+434.25778x^8-222.07709x^9

R^2=0.9998 SD= 1.7936

Complex **4** $[Er_2(2\text{-Br-5-MOBA})_6(phen)_2]$ (T=263.15 K to 456.15 K)

$C_{p,m}/J\cdot mol^{-1}\cdot K^{-1}$=1234.01261+95.24482$x-35.43295x^2$+945.06973$x^3-839.14337x^4-1238.24804x^5$+1359.51675$x^6$+522.40198$x^7-617.5879x^8$+11.10152$x^9$

R^2=0.9996 SD= 3.68064

T represents the experimental temperature, T_{max} represents the highest temperature and T_{min} represents the lowest temperature. Besides, R^2 represents the correlation coefficient and SD represents the standard deviation. [37]

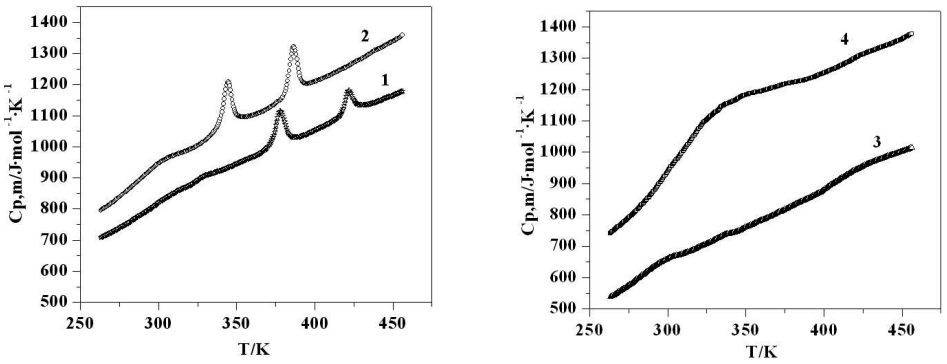

(a) **(b)**

Fig. 3 Molar heat capacity along with the change of temperature curve of complexes **1**,**2**(a) and **3**,**4**(b)

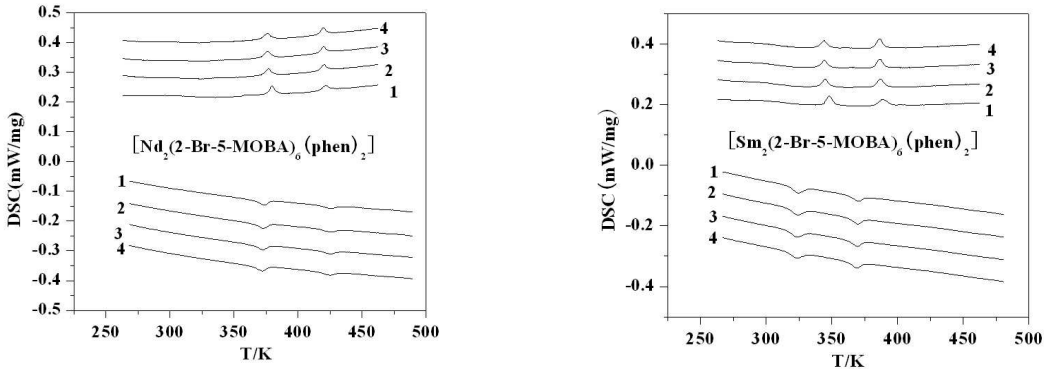

(a) **(b)**

Fig. 4 DSC curves of four thermal circulating processes of complexes **1**(a) and **2** (b)

Table 7 Data of the circulating processes in the heating and cooling processes for complexes **1** and **2** (I and II representative the data of the first and second phase transition , respectively.)

Complexes	circulating processes		Heating process				Cooling process			
			$T_{0(K)}$	$T_{P(K)}$	$T_{t(K)}$	Endothermic (KJ/mol)	$T_{0(K)}$	$T_{P(K)}$	$T_{t(K)}$	Exothermic (KJ/mol)
1	1	I	376.34	379.69	381.93	1.652	352.60	355.33	358.19	-0.991
		II	417.50	421.21	424.30	0.914	395.20	400.86	403.19	-0.599
	2	I	372.82	376.94	379.60	1.503	348.45	355.24	358.59	-0.990
		II	416.38	419.96	423.08	0.902	393.66	400.46	402.85	-0.662
	3	I	371.95	376.79	379.55	1.410	351.55	354.81	358.27	-0.893
		II	416.94	420.06	422.72	0.958	396.60	400.56	400.76	-0.628
	4	I	371.82	376.02	379.11	1.361	350.75	355.00	357.50	-0.851
		II	416.33	419.31	422.07	0.959	395.20	400.44	404.74	-0.603
2	1	I	344.01	347.97	351.42	1.813	309.98	315.38	321.12	-1.747
		II	384.14	388.48	392.78	1.740	352.37	357.26	360.91	-1.140
	2	I	341.02	344.66	348.06	1.657	310.43	314.80	319.96	-1.650
		II	379.89	386.84	390.07	1.892	352.54	356.38	361.00	-1.133
	3	I	340.28	344.47	347.68	1.672	309.49	314.59	320.60	-1.655
		II	381.92	386.14	390.23	1.932	352.47	356.49	360.02	-1.100
	4	I	339.63	343.58	347.52	1.651	306.43	314.41	317.41	-1.696
		II	382.48	386.40	389.77	1.989	350.4	356.17	359.62	-1.116

T_0 is the initial temperature of the phase transition peak by DSC extrapolation;

T_t is the ending temperature of the phase transition peak by DSC extrapolation;

T_p is the peak temperature of the phase transition peak.

Luminescence spectrum of complex 2

The solid state luminescence property for complex **2** is investigated at room temperature. The excitation spectrum of complex **2** with the emission wavelength of 598 nm was presented in Fig. 5(a). As seen from Fig. 5(a), there are two obvious peaks at 340-400 nm and 484 nm. The band at 340 nm to 400 nm is likely to be attributed to charge transfer band (CT band) from ligand to center metal. The characteristic emission spectrum of Sm^{3+} ion is observed under the excitation wavelength of 484 nm as shown in Fig.5(b). The typical emission peaks of Sm^{3+} ion occur at 565 nm, 598 nm and 645 nm. The characteristic peaks can be attributed to the following transitions of Sm(III) ion:$^4G_{5/2}\rightarrow{}^6F_{5/2}$, $^4G_{5/2}\rightarrow{}^6F_{7/2}$ and $^4G_{5/2}\rightarrow{}^6F_{9/2}$, respectively, [38] suggesting the complex **2** will be an excellent candidate for luminescent material.

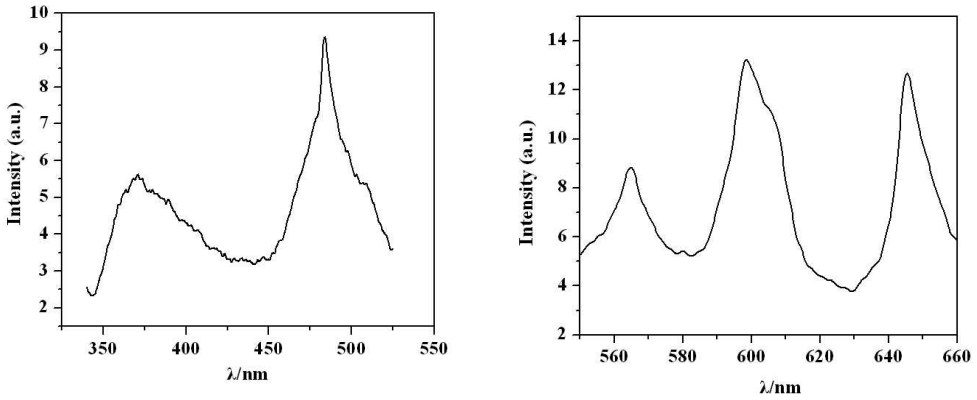

(a) (b)

Fig. 5 The excitation spectrum (a) and emission spectrum (b) of complex **2** (**λ_{em}**=598 nm, **λ_{ex}**=484 nm**)**

Bacteriostatic activity

The experimental conditions: the filter diameter is 6 mm. The sample volume of complexes is 5 uL, and the concentration of complexes are 8×10^{-3} mol/L, 16×10^{-3} mol/L and 32×10^{-3} mol/L, respectively. Temperature is 30 ℃. The bacteriostatic activities of complexes **1** - **4** to *candida albicans, escherichia coli, and staphylococcus*

Table 8 The bacteriostatic activities of complexes **1** to **4** to candida albicans

Complexes	Concentration gradient(mol/L)	The diameter of bacteriostatic ring for three times in parallel (mm)			Average(mm)	The standard deviation(mm)
		Ⅰ	Ⅱ	Ⅲ		
	8×10^{-3}	13.60	14.00	13.80	13.80	0.38
1	16×10^{-3}	24.40	25.00	25.30	24.90	0.46
	32×10^{-3}	30.90	31.60	31.00	31.17	0.20
	8×10^{-3}	14.10	14.50	14.20	14.27	0.42
2	16×10^{-3}	17.30	17.00	17.70	17.33	0.35
	32×10^{-3}	29.20	29.00	29.80	29.33	0.21
	8×10^{-3}	12.30	11.70	12.10	12.03	0.57
3	16×10^{-3}	24.50	23.70	25.00	24.40	0.66
	32×10^{-3}	28.90	29.70	30.00	29.53	0.31
	8×10^{-3}	15.70	16.50	16.30	16.17	0.44
4	16×10^{-3}	21.30	21.00	21.90	21.40	0.46
	32×10^{-3}	31.40	31.50	30.70	31.20	0.42

aureus are determined. Complexes **1** to **4** almost have no bacteriostatic action to the latter two bacteria, but they have good bacteriostatic action to *candida albicans*(fungi). We inferred that bacteria and fungi had different composition and structure of the cell walls, which leaded to the result. The diameter of bacteriostatic ring with the different

concentration of complexes **1-4** are listed in Table 8, and the corresponding column diagram is shown in Fig.6. The diameter of bacteriostatic ring of a reference blank (DMSO only) with the different concentration is 6mm. As seen from the Table 8, bacteriostatic ring diameter of complexes **1** to **4** are all bigger than the filter diameter (6mm), which prove that the complexes have good bacteriostatic action to *candida albicans*.[39,18] Besides, as seen from Fig. 6, the bacteriostatic action are more and more remarkable with the increase of concentration.

Because the concentration of the complex was higher, the bacteriostatic effect was more obvious during the minimum concentration range. Totally, lanthanide complexes has certain bacteriostatic actions against microorganism，which has commonly been explained that Ln(III) ions are coordinated with the donor atoms of the ligands. This leads to the π-electron delocalization over the chelate ring further to reduces the polarity of the central metal ion. The phenomenon in turn favors permeation to the lipid layer of the membrane for lanthanide complexes.[40-41]

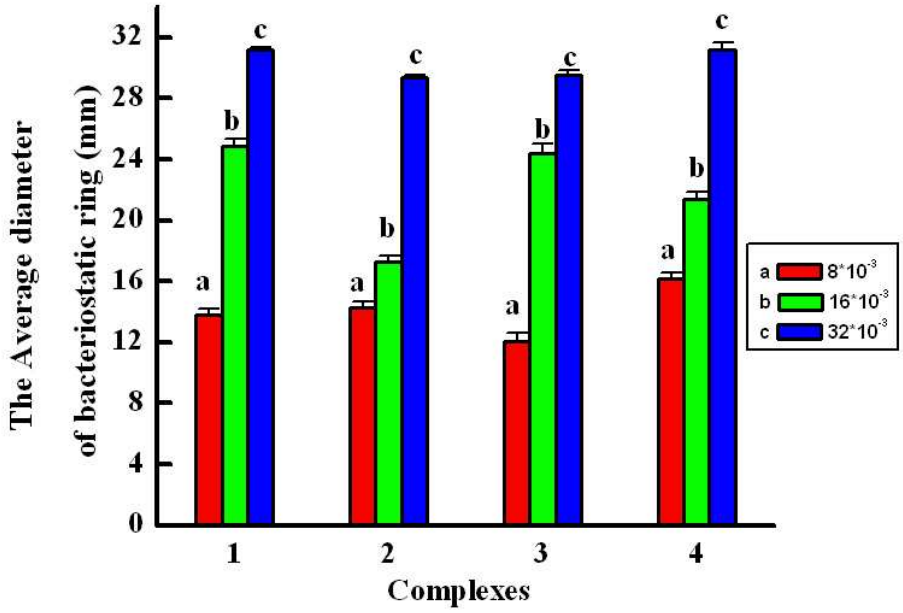

Fig. 6 The bacteriostatic activities of complexes **1** to **4** to candida albicans

Magnetic properties of complexes 3 and 4

The variable temperature magnetic susceptibilities for complexes **3** and **4** are determined with an applied magnetic field of 1000 Oe in the temperature range of 2 to 300 K. The plots of $\chi_M T$ *vs.* T and χ_M^{-1} *vs.* T are given in Fig. 7. For complex **3**, the value

of $\chi_M T$ is 28.03 $cm^3 \cdot K \cdot mol^{-1}$ at room temperature, which is close to the calculated value of 28.14 $cm^3 \cdot K \cdot mol^{-1}$ for two uncoupled Ho(III) ions in the $^5I_8$ state. [41-42] With the decrease of temperature, the $\chi_M T$ value gradually reduces to 9.27 $cm^3 \cdot K \cdot mol^{-1}$ at 2 K. It obeys the Curie–Weiss Law over the whole temperature range with a Curie constant of C = 28.59 $cm^3 \cdot K \cdot mol^{-1}$ and Weiss constant of θ = –8.16 K. For complex **4**, the $\chi_M T$ value is 27.89 $cm^3 \cdot K \cdot mol^{-1}$ at room temperature, which is higher than the calculated value of 22.96 $cm^3 \cdot K \cdot mol^{-1}$ for two uncoupled Er(III) ions in the $^4I_{15/2}$ state. [42] With the decrease of temperature, the $\chi_M T$ value smoothly decreases to a minimum of 9.24 $cm^3 \cdot K \cdot mol^{-1}$ at 2 K. The corresponding Curie and Weiss constant are 25.89 $cm^3 \cdot K \cdot mol^{-1}$ and -9.58 K, respectively. For the Ho(III) and Er(III) complexes, it's difficult to carry out a theoretical treatment of magnetic interactions due to the spin-orbit coupling of Ln(III). The decreases of $\chi_M T$ for products are the comprehensive results, including the magnetic exchange interaction between spin bearers and the depopulation of the Stark sub-levels associated with the crystal field effects. [44]

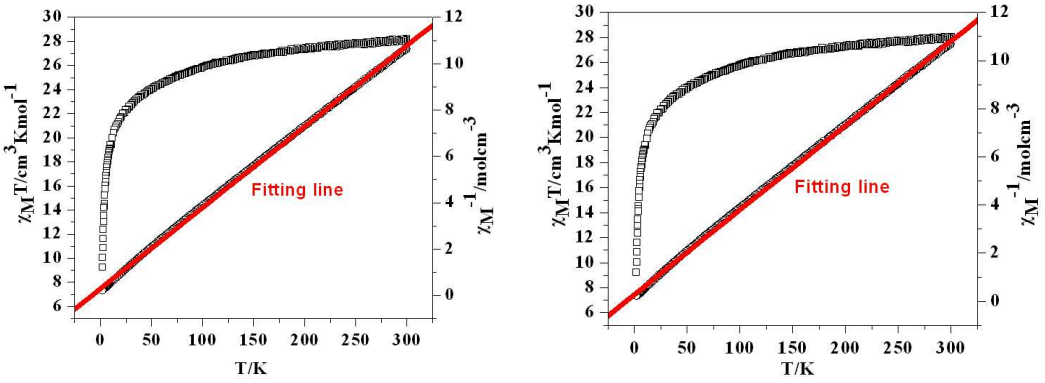

(a) **(b)**

Fig. 7 $\chi_M T$ *vs* T(the hollow box) and χ_M^{-1} *vs* T(the hollow circle) of complexes **3**(a) and **4**(b) (The red line : fitting line)

Conclusion

Four kinds of new lanthanide complexes with the formula $[Ln_2(2\text{-Br-5-MOBA})_6(phen)_2]$ (Ln=Nd(**1**), Sm(**2**), Ho(**3**), Er(**4**)) were synthesized. These complexes were isostructural and nine coordinated. Complexes **1** to **4** were stable up to 500 K by thermogravimetric analysis. The average molar heat capacity value of

the complexes ($C_{p,m}/(J\cdot K^{-1}\cdot mol^{-1})$) gradually increased with the increasing of temperature (T/K) just for complexes **3** and **4**. Both complexes **1** and **2** contained two solid–solid phase transitions at different temperature range. Among the three transitions of fluorescence spectrum for complex **2**, located in the 598nm was the strongest which belonged to the characteristic transitions of Sm(III) ion, $^4G_{5/2}\rightarrow{}^6F_{7/2}$. All the complexes had good bacteriostatic action to candida albicans. The magnetic investigation indicates that the $\chi_M T$ products of Ho (III) and Er (III) complexes decrease upon cooling. This behavior results from the magnetic exchange interaction between spin bearers and the depopulation of the Stark sub-levels associated with the crystal field effects.

Supporting Information

CCDC1023976, CCDC1023986, CCDC1023985 and CCDC1023983 contain the supplementary crystallographic data for $[Nd_2(2\text{-Br-5-MOBA})_6(phen)_2]$(**1**), $[Sm_2(2\text{-Br-5-MOBA})_6(phen)_2]$(**2**), $[Ho_2(2\text{-Br-5-MOBA})_6(phen)_2]$(**3**), $[Er_2(2\text{-Br-5-MOBA})_6(phen)_2]$(**4**).These data can be obtained free of charge from The Cambridge Crystallographic Data Centre at www.ccdc.cam.ac.uk/data_request/cif. This material is available free of charge via the Internet at http://pubs.rsc.org. The average molar heat capacity values of the complexes **1**, **2** and **3**, **4** were shown in Table S1 and S2.

Acknowledgments

The research work is supported by the National Natural Science Foundation of China (No. 21073053，21473049) and the Natural Science Foundation of Hebei Province (No. B2012205022).

Rreferences

[1]P.S. Koroteev, M.A. Kiskin, Zh.V. Dobrokhotova, A.S. Bogomyakov, N.N. Efimov and V.M. Novotortsev, *Polyhedron.,* **2011**, 30, 2523.

[2]K.M. Buschbaum and C.C. Quitmann, *Inorg. Chem.,* **2006**, 45(6), 2678.

[3]A.M.Zhu, Q.Y.Jin, D.X.Jia, J.S.Gu and Y.Zhang, *Eur. J. Inorg . Chem.,* **2008**, 30, 4756.

[4]N.K. Al-Rasb, H. Adams and F.O. Suliman, *Dyes Pigments.,* **2014**, 104, 83.

[5]J.Z. Gu, J. Wu, D.Y. Lv, Y. Tang, K.Y. Zhu and J.C. Wu, *Dalton Trans.,* **2013**, 42, 4822.

[6]L.R. Yang, L. Liu, L.Z. Wu, Z.H. Xu and L.Wang, *Dyes Pigments.,* **2014**, 111, 176.

[7]J.C.G. Bünzli, *Accounts .Chemi.Res.,* **2006**, 39, 53.

[8]L.F. Li, D.B. Dong, J.Y. Zhang, C.N. Zhang and G.Jia, *Mater.Lett.,* **2014**, 131, 300.

[9]Y.S. Zhou, X.M. Li, L.J. Zhang, Y. Guo and Z.H. Shi, *Inorg. Chem.,* **2014**, 53, 3368.

[10]W.T. Chen and S. Fukuzumi, *Inorg. Chem.,* **2009**, 48, 3805.

[11]R. Sessoli and A.K. Powell, *Coordin.Chem.Rev.,* **2009**, 253, 2335.

[12]F.M. Zhang , P.F. Yan, X.Y. Zou, J.W. Zhang , G.F. Hou and G.M. Li, *Cryst. Growth Des.,* **2014**, 14 (4), 2014.

[13]J. Goura, J.P.S. Walsh, F. Tuna and V. Chandrasekhar, *Inorg. Chem.,* **2014**, 53, 3385.

[14]A. Rossin, G. Giambastiani, M. Peruzzini and R. Sessoli, *Inorg. Chem.,* **2012**, 51, 6962.

[15]J.Q. Bao, Z.F. Zhang, R.R. Tang, H.X. Han and Z.F. Yang, *J.Lumin.,* **2013**, 136, 68.

[16]I.G. Fomina, Z.V. Dobrokhotova, G.G. Aleksandrov, V.I. Zhilov, I.P. Malkerova, A.S. Alikhanyan, D.M. Zhigunov, A.S. Bogomyakov, V.I. Gerasimova, V.M. Novotortsev and I.L. Eremenko, *Polyhedron.,* **2013**, 50, 297.

[17]B. Yue, H.J. Sun, Y.N. Chen, K. Kong, H.B. Chu and Y.L. Zhao, *Appl. Organomet. Chem.*, **2014**, 28, 167.

[18]Q.Z. He, J. Yang, H. Min and H.X. Li, *Mater.Lett.,* **2006**, 60, 320.

[19]S.Z. Tan, L.L. Zhang, L.Y. Xia,Y.S. Liu and D.X. Li, *T. Nonferr. Metal. Soc.,* **2007**, 17, 260.

[20]A.B. Siqueira, G. Bannach, E.C. Rodrigues, C.T. Carvalho and M.Ionashiro, *J. Therm.Anal.Calorim.,* **2008**, 91 (3), 897.

[21]W. Ferenc and A. Walków-Dziewulska, *J.Therm.Anal.Calorim.,* **2002**, 70, 949.

[22]W. Brzyska and W. Ożga, *J.Therm.Anal.Calorim.,* **2004**, 78, 999.

[23]W. Ferenc and B.Bocian, *J.Therm.Anal.Calorim.,* **2000**, 60, 131.

[24]S. Raphael, M.L.P. Reddy, K.V. Vasudevan and A.H. Cowley, *Dalton Trans.,* **2012**, 41, 14671.

[25]D.F. Lu, Y.Y. Di, Z.C. Tan and J.M. Dou, *J.Therm.Anal.Calorim.,* **2013**, 111, 216.

[26]K. Tang, H.M. Liu, N. Ren, J.J. Zhang and K.Z. Wu, *J.Chem.Thermodyn.,* **2012**, 47,

434.

[27] J.F. Wang, F.T. Meng, S.L. Xu, X. Liu, J.J. Zhang, *Thermochim. Acta*., **2011**,521, 2.

[28]J. F. Wang, H. Li, J.J. Zhang, N. Ren and K.Z. Wu, *Sci.China.Chem.,* **2012**, 55 (10), 2162.

[29]Z.H. Yang, J. Xu, W.X. Zhang, A.P. Liu and S.P. Tang, *J.Solid. State. Chem.,* **2007**, 180, 1391.

[30]W.J. Geary, *Coordin.Chem.Rev.,* **1971**, 7, 94.

[31]H.W. Gu, S.X. Xiao, H.Y. Xiao, Y. Xiao, A. T.Li, X.L. Hu and Q.G.Li, *Ind. Eng.Chem.Res.,* **2012**, 51, 4800.

[32]B.L. An, M.L. Gong, M.X. Li and J.M. Zhang, *J.Mol.Struct.,* **2004**, 687, 4.

[33]J.F. Wang, N. Ren, J.J. Zhang, K.Z. Wu and S.P. Wang, *J.Chem.Eng.Data.,* **2010**, 55, 4983.

[34]R. Feng, F.L. Jiang, M.Y. Wu, L. Chen, C.F. Yan and M.C. Hong, *Cryst. Growth Des.,* **2010**, 10(5), 2308.

[35]D.A. Bardwell, J.C. Jeffery, P.L. Jones, J.A. McCleverty, E. Psillakis, Z. Reeves and M.D. Ward, *J. Chem. Soc. Dalton Trans*., **1997**, 2082.

[36]R. Łyszczek, Z. Rzączyńska, A. Kula and A. Gładysz-Płaska, *J.Anal.Appl.Pyrol.*, **2011**, 92, 347.

[37]J.N. Zhang, H. Wang, Z.C. Tan, B.P. Liu, Q. Shi and B. Tong, *J.Rare.Earth.,* **2009**, 27(6), 921.

[38]W.X. Li, S.Y. Feng, Y. Liu, J. Zhang, X.D. Xin, B.Y. Ao and Y.J. Li, *J.Lumin.,* **2013**, 143, 750.

[39]H. Yu, Q.Z. He, J. Yang and W.J. Zheng, *J.Rare.Earth.,* **2006**, 24, 4.

[40]J. Hang, Y.H. Xu, X.K. Chen, D.F. Xu, Y.M. Xu and Q.Z. He, *J.Rare.Earth.,* **2012**, 30 (6), 586

[41]Y.F. Zhao, H.B. Chu, F. Bai, D.Q. Gao, H.X. Zhang, Y.S. Zhou, X.Y. Wei, M.N. Shan, H.Y. Li and Y.L. Zhao, *J. Organomet. Chem.,* **2012**, 716, 167.

[42]C. Benelli and D. Gatteschi, *Chem.Rev.,* **2002**, 102, 2370.

[43]Z.J. Lin, B. Xu, T.F. Liu, M.N. Cao, J. Lü and R. Cao, *Eur.J. Inorg.Chem.,* **2010**, 24,

3847.

[44]L. Norel, L.M. Chamoreau, Y. Journaux, O. Oms, G. Chastanet and C. Train, *Chem.Commun.,* **2009**, 2382.